DOI: 10.1002/cphc.200600110

Asymmetry Induction by Cooperative Intermolecular Hydrogen Bonds in Surface-Anchored Layers of Achiral Molecules**

Alexandre Dmitriev,*[a] Hannes Spillmann,[a] Sebastian Stepanow,[a] Thomas Strunskus,[b] Christof Wöll,[b] Ari P. Seitsonen,[c] Magali Lingenfelder,[a] Nian Lin,*[a] Johannes V. Barth,*[d, e] and Klaus Kern[a, e]

The mesoscale induction of two-dimensional supramolecular chirality (formation of 2D organic domains with a single handedness) was achieved by self-assembly of 1,2,4-benzenetricarboxylic (trimellitic) acid on a Cu(100) surface at elevated temperatures. The combination of spectroscopic [X-ray photoelectron spectroscopy (XPS) and near-edge X-ray absorption fine structure (NEXAFS)], real-space-probe [scanning tunneling microscopy (STM)], and computational [density functional theory (DFT)] methods allows a comprehensive characterization of the obtained organic adlayers, where details of molecular adsorption geometry, intermolecular coupling, and surface chemical bonding are elucidated. The trimellitic acid species, comprising three functional carboxylic groups, form distinct stable mirror-symmetric hydrogen-bonded domains. The chiral ordering is associated with conformational restriction in the domains: molecules anchor to the substrate with an ortho *carboxylate group, providing two* para *carboxylic acid moieties for collective lateral interweaving through H bonding, which induces a specific tilt of the molecular plane. The ease of molecular symmetry switching in domain formation makes homochiral-signature propagation solely limited by the terrace width. The molecular layer modifies the morphology of the underlying copper substrate and induces μm-sized strictly homochiral terraces.*

Introduction

The subject of spontaneous symmetry breaking is of fundamental interest in view of the ubiquitous presence of chirality in nature. Besides its importance in life sciences, a rich variety of chiral phenomena occurs in surface processes, and issues of general importance for chiral order evolution, such as spontaneous separation (resolution) or chirality induction in the assemblies, can be successfully addressed in two-dimensional systems. Moreover, producing surfaces with chiral signature is of practical interest due to their selective response when interacting with adsorbed species, whence their stereochemical properties can be exploited for enantio-selective heterogeneous catalysis and ultra-sensitive molecular detection. Several methodologies are exploited for the preparation of chiral surfaces: Using their intrinsic crystallographic symmetry (such as high-index chiral metal surfaces[1–3]); adsorbing chiral[4–12] or pro-chiral (two-dimensionally chiral)[13–19] molecular species, which become chiral by mirror-symmetry breaking upon 2D confinement on a substrate, and by the respective combinations—for example, by molecular asymmetric restructuring of the substrate,[20,21] by coadsorption of achiral and chiral species,[12,22] or by using the electrodeposition technique in the presence of chiral molecular ions.[23] Moreover, chirality can be achieved at the supramolecular level by the assembly of either achiral, prochiral or chiral molecular building blocks in architectures implying symmetry breaking.[24–26]

[a] *Dr. A. Dmitriev,[+] Dr. H. Spillmann, Dr. S. Stepanow, M. Lingenfelder, Dr. N. Lin, Prof. K. Kern*
Max-Planck-Institut für Festkörperforschung
70569 Stuttgart (Germany)
Fax: (+49) 711-689-1662
E-mail: alexd@fy.chalmers.se
n.lin@fkf.mpg.de

[b] *Dr. T. Strunskus, Prof. C. Wöll*
Lehrstuhl für Physikalische Chemie I, Ruhr-Universität Bochum
44780 Bochum (Germany)

[c] *Dr. A. P. Seitsonen*
CNRS & IMPMC, Université Pierre et Marie Curie
4 place Jussieu, case 115, 75252 Paris (France)

[d] *Prof. J. V. Barth*
Departments of Chemistry and Physics & Astronomy
University of British Columbia, Vancouver, BC V6T 1Z4 (Canada)
Fax: (+1) 604-822-4750
E-mail: jvb@chem.ubc.ca

[e] *Prof. J. V. Barth, Prof. K. Kern*
Institut de Physique des Nanostructures
Ecole Polytechnique Fédérale de Lausanne, 1015 Lausanne (Switzerland)

[+] *Current Address:*
Applied Physics, Chalmers University of Technology
41296 Göteborg (Sweden)
Fax: (+46) 31-772-3134

[**] *A Combined X-ray Photoelectron Spectroscopy, Near-Edge X-ray Absorption Fine Structure, Scanning Tunneling Microscopy, and Density Functional Theory Study of the Mesoscopic Organization of Homochiral Trimellate Layers on Cu(100).*

Herein, we demonstrate spontaneous chirality induction on a metal surface by the formation of highly ordered assemblies, with a single handedness on the μm scale, stabilized by combined metal–organic and H-bonding interactions. We employ a single 3D achiral molecular component, the polycarboxylic acid (1,2,4-benzenetricarboxylic acid, tmla) adsorbed on a fourfold symmetric Cu(100) substrate to demonstrate that mesoscopic organization of chiral organic adlayers can be obtained on a highly symmetric substrate as a result of the interplay of substrate–adsorbate and intermolecular interactions. Trimellitic acid possesses an asymmetric molecular geometry, with carboxylic functionalities at *ortho* and *para* positions which make the molecule prochiral, that is, two-dimensional confinement in a flat geometry leads to chirality induction (see Figure 1a). The molecule is known to form various hydrogen-bonded architectures, where its asymmetric molecular structure leads to particular topologies.[27] Its closest structural analogue—terephthalic (1,4-benzenedicarboxylic) acid—with functional groups only in *para* positions was recently shown to form 2D H-bonded sheets at metal surfaces, where the molecules are bond in a flat-lying geometry.[28–31] In previous investigations we have demonstrated how metal–organic complexation can be explored to bestow chiral asymmetry to metal surfaces using this and related species.[32,33] Also, the prochiral tmla can be used to build a series of metallosupramolecular architectures, where the carboxylate functionalities play a key role in the evolution of two-dimensional chiral order or network formation.[34–36] Additionally, it has been shown that molecules with two- or threefold exodentate carboxylic functionality may also adopt an upright geometry upon carboxylate coupling to metal substrates, exposing their carboxylic functional groups for noncovalent intermolecular interactions.[37,38]

The complexity of the tmla/Cu(100) system requires a combined analysis using complementary surface-sensitive probes with ab intio calculations to conclusively characterize bonding, conformational orientation, and two-dimensional chiral ordering in the supramolecular layer. X-ray photoelectron spectroscopy (XPS) was employed to identify the chemical nature of the adsorbed species by monitoring the temperature- and coverage-dependent evolution of the C1s and O1s core-level photoemission signals, indicating partial deprotonation of the carboxyl groups and formation of a monocarboxylate species. A near-edge absorption fine structure (NEXAFS) analysis allows the determination of the molecular orientation in the supramolecular architecture, where a substantial out-of-plane tilt of the molecular plane was detected. Scanning tunneling microscopy (STM) measurements reveal the very chiral nature and mesoscopic ordering in the organic layers, as well as their long-range periodicity and commensurability with the underlying Cu(100) substrate. Moreover, in the STM data, changes in the surface morphology become apparent, that is, μm-sized homogenous substrate terraces develop in the evolution of the molecular layer. Finally, details of surface chemical bonding, molecular conformation, and intermolecular interactions in the domains, leading to chirality induction, are addressed by density functional theory (DFT) calculations.

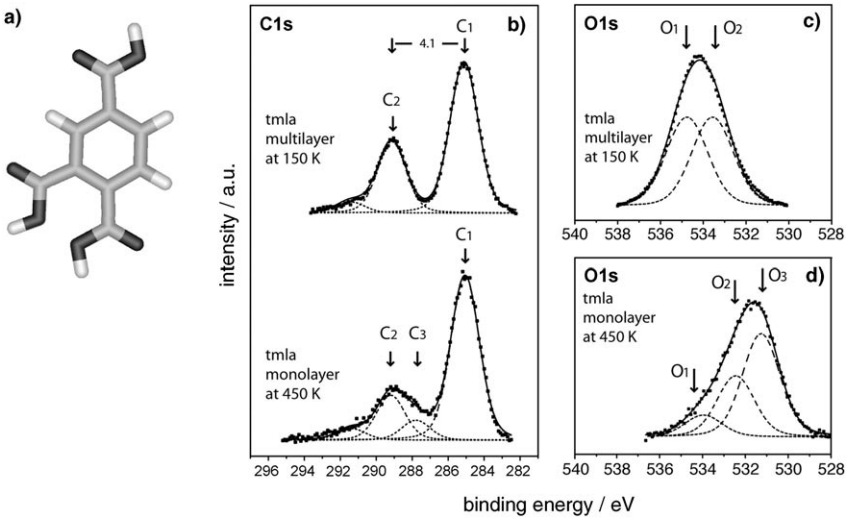

Figure 1. Photoemission spectra of the C1s and O1s levels for tmla layers on Cu(100). a) The integral molecule comprises three carboxylic groups, as shown in the chemical structure model (carbon backbone shown in light grey, oxygen atoms in dark grey, hydrogen atoms in white). b) Evolution of C1s in the high-temperature adlayer preparation. Upper part: tmla multilayer prepared on a substrate held at low temperature (150K). The characteristic peaks, assigned to phenyl (C1) and carboxyl (C2) carbons, are separated by 4.1 eV. Lower part: tmla monolayer deposited at 450K. Whereas the phenyl-carbon peak (C1) remains unchanged, the carboxyl splits in two and a new peak—separated from C1 by 3 eV and assigned to a carboxylate moiety (C3)—develops. For clarity, the multilayer spectrum is normalized with the lower one to eliminate multilayer–monolayer energy shifts. c) and d) O1s region for multilayer (b) and monolayer (c) depositions. The full-width at half-maximum (fwhm) parameters for fitting Voigt curves are 2.27 and 2.06 eV for multilayers and monolayers, respectively. Two identical fitting curves for the broad oxygen peak at 150K are assigned to hydroxyl (O1) and carbonyl (O2) oxygen atoms, while the sharp peak (O3) appearing upon 450K preparation is associated with both carboxylate (copper–carboxylate) and carbonyl oxygen atoms involved in lateral H bonding in the domain.

Results and Discussion

To address the chemical nature of the adsorbed species, XPS experiments were performed both for multi- and monolayer thickness. The C1s spectrum for multilayer deposition (obtained at 150K) shown in the upper part of Figure 1b confirms that tmla carboxyl groups remain largely complete, that is, the well-known splitting of the C1s peak is observed, reflecting the contribution from the atoms in the carboxyl and phenyl moieties (marked as C_2 and C_1 in Figure 1b, respectively).[39–43] This characteristic separation of the two peaks (around 4 eV) for related carboxylic acids has been documented in the literature.[44] The fitted Voigt function gives an intensity phenyl-to-carboxyl ratio of 2:1, in agreement with the molecular stoichiometry. Accordingly, the O1s peak (Figure 1c) appears broadened due

to overlapping hydroxyl and carbonyl intensities [absolute values for deconvoluted lines are 533.2 (O_1) and 534.4 eV (O_2), respectively]. The corresponding NEXAFS analysis of the multilayer phase shown in Figure 2 indicates that adsorption with the aromatic ring largely parallel to the substrate (average tilt angle of $60\pm5^\circ$ with respect to the surface normal) prevails for the entire overlayer. Consequently, a hydrogen-bonded organic molecular film develops with a structure presumably similar to that encountered for the tmla crystalline phase.[45] A tentative assignment for the NEXAFS resonances indicated in the spectra is summarized in Table 1; these resonances are in overall agreement with previous observations on the phenylacetylene/Cu(100) system.[46]

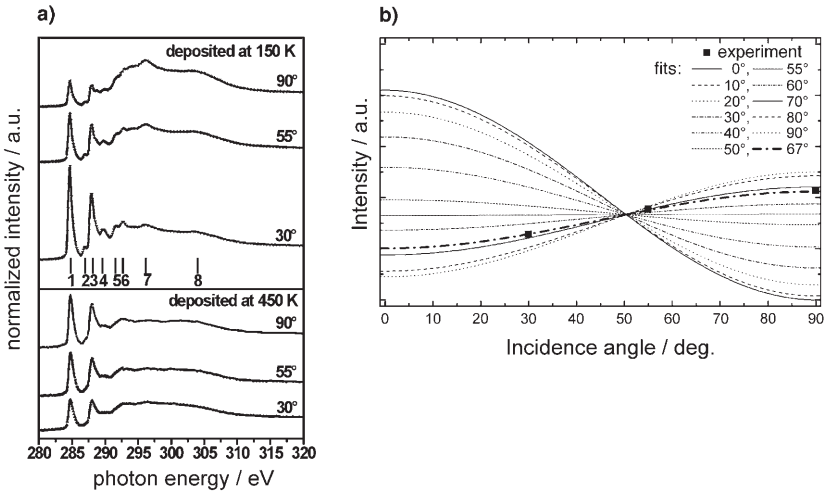

Figure 2. a) NEXAFS spectra recorded at the C K edge for a tmla multilayer prepared at 150 K (upper graph, measured at the deposition temperature) and at 450 K (measured at room temperature). The different lines indicate spectra obtained at different angles of incidence of the synchrotron light [90° means normal incidence to the Cu(100) surface]. Different contributions are marked; for the assignment, see text and Table 1. b) Extraction of the value for the tilt of the molecular plane from the NEXAFS intensity data for the monolayer tmla coverage. The best fit is obtained with a tilt of 67 ± 5 degrees (23 ± 5 degrees from the surface normal).

Drastic changes occur in the adsorption scenario when the molecules are deposited on the substrate held at 450 K. The STM data discussed below confirm that this procedure results in the formation of a homogenous tmla monolayer (ML), which is similarly reflected by the decrease of absolute intensities for both C1 s and O1 s peaks. Moreover, the C1 s XPS data (see Figure 1 b, lower part) evidence the split of the carboxyl peak in two contributions. An additional peak evolves at lower binding energy (marked C_3 in Figure 1 b, 287.6 eV) compared to the carboxyl line (C_2, 288.9 eV) and is about 3 eV separated from the phenyl peak (284.8 eV). Consequently, it is assigned to carboxylate formation, which agrees well with the peak shifts reported in the literature.[47–49] The ratio of carboxyl to carboxylate, extracted from fitted curves, amounts to 2:1, which indicates that only one out of three tmla carboxylic functionalities becomes deprotonated in the process of adlayer formation at elevated temperature. Furthermore, a remarkable change in the peak shape is apparent in the O1 s spectrum of this phase (Figure 1 d). A drastic asymmetric decrease of the hydroxyl peak (O_1) is accompanied by the evolution of a new dominant peak at 531.2 eV (marked O_3), which is, again, associated with deprotonation of a carboxylic group. The latter substantially increases the coupling to the substrate, which is known for carboxylates on chemically reactive metal substrates (see Dmitriev at al.[38] and references therein). The ionization of a carboxylic moiety, Cu–carboxylate bond formation, and lateral H bonding substantially affect the charge-density distribution in the tmla: A feasible scenario for the overall decrease of the hydroxyl oxygen contribution and the dominance of the newly developed peak at low binding energy (Figure 1 d) can be the shift of one of the hydroxyl and one of the carbonyl oxygen species to lower binding energies due to a partial increase of the electronic density. With such shifts, only one hydroxyl oxygen would contribute to the O_1 peak, along with one carboxyl and one hydroxyl oxygen species contributing to the O_2 peak. The rest of the oxygen species (a carbonyl and two carboxylates) would be responsible for the O_3-peak dominance in the O1 s spectrum. The charge-redistribution scenario upon tmla deprotonation (tmla binding to the substrate and, laterally, to the neighboring species is largely supported by the DFT calculations) is discussed below. Overall, we can conclude, that the organic monolayer is composed of monotrimellate species anchored to the substrate with a single carboxylate functionality, leaving the remaining two carboxylic moieties available for lateral intermolecular coupling.

Table 1. Assignment of the NEXAFS resonances.

Resonance	Energy [eV]	Assignment
1	284.8	C(Ph)→π*(Ph)
2	287.0	π*
3	288.2	C(COOH))→π*(COOH), C(Ph)→π*(Ph, COOH)
4	289.6	Rydberg
5	291.6	π* and σ*
6	292.7	π* and σ*
7	296.2	σ*
8	304	σ*

The C K-edge NEXAFS spectra of tmla monolayers recorded at selected X-ray incidence angles are presented in the lower part of Figure 2 a. The tentative assignment of the NEXAFS resonances is summarized in Table 1. The spectra show two main peaks associated with bound resonances.[50] The pronounced peak at about 284.8 eV is attributed to a characteristic C1 s–π* resonance for the aromatic ring system, whereas the resonance

at 288.2 eV is attributed mainly to the C1 s–π* transition of the carboxyl groups. In the spectra recorded for the monotrimellate monolayer, the C1 s–π* resonances show only a small intensity variation with the angle of incidence, whereby the 90° spectrum has the largest intensity. This corresponds either to an almost random orientation of the molecules or to a situation were the plane of the tmla is oriented, on average, at a tilt angle of approximately 67 ± 5 degrees relative to the Cu(100) surface (23 ± 5° from the surface normal), as shown in Figure 2b (details of the NEXAFS angular-dependence fit are described in the Experimental Section). The latter is consistent with a partial deprotonation of the tmla molecule, where only one of the three functional groups is engaged in the carboxylate-mediated anchoring to the substrate and the formation of a homogenous organic layer, as described below. Hence, we interpret the NEXAFS data in terms of a (≈25°) tilted monotrimellate species.

To gain a real-space insight into both structural details and mesoscopic ordering of the tmla monolayers obtained upon 450 K deposition, STM experiments were conducted. An overview image of the tmla adlayer is presented in Figure 3, where the width of the individual surface terraces amounts to 10 nm or less. The step–terrace reconstruction of the surface covered with the organic layer is thus clearly distinct from that of the pristine substrate, where no step bunching is encountered and terraces are usually more regular in width. Consequently, the molecular ordering that arises locally upon tmla domain evolution by molecular self-assembly extends to the mesoscopic scale through formation of vast μm-sized stripes. Thus, the domain formation goes along with massive copper-surface mass transport. This is in agreement with previous observations of strong noble-metal-surface modification upon adsorption of organic species,[51–53] resulting in step–edge faceting and bunching.[54–56] An analysis of the STM data with sub-monolayer tmla coverages (coverages below 0.5 ML, data not shown) provides evidence of substantial modifications of the step–edge shape in the terraces, where the ordered domains start to develop.

In the high-resolution STM images reproduced in Figure 4 the local organization and homogenous asymmetric nature of the organic layer are resolved. Two distinct types of well-or-

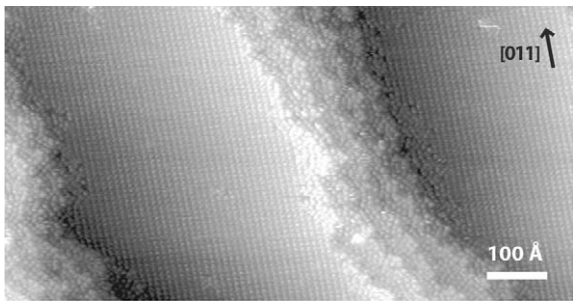

Figure 3. STM image providing a view of the Cu(100) surface morphology modified under the influence of the trimellate monolayer deposited at 450 K. The structure of the regular adlayer domains, oriented along the Cu [011] direction, can be seen in the large terraces. Irregular tmla aggregates exist on bunches of narrow terraces.

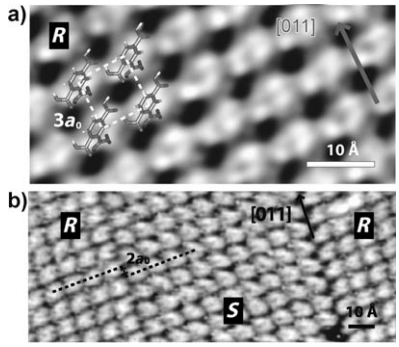

Figure 4. Chiral nature of the trimellate domains. The submolecular-resolution STM data show individual tmla species appearing as three-lobe protrusions organized in an asymmetric, repetitive pattern, defined as *R*-type domain. a) The structural model of chirally conformed tmla, forming the *R* domain, and a (3×3) superstructure unit cell are depicted [Cu(100) nearest-neighbor distance: $a_0 = 2.55$ Å]. b) STM image showing the rare case of boundaries between two homochiral domains in a terrace (marked as *R* and *S*). The domain wall, coinciding with the Cu [011] azimuth, represents the mirror symmetry axis. In the neighboring domains, molecules are shifted by $2a_0$ (2×2.55 = 5.1 Å) in the direction of the marked copper azimuth.

a remarkable reshaping of the surface morphology becomes apparent. In striking contrast to the regularly terraced pristine substrate, extremely wide and elongated terraces have been developed, which alternate with bunches of narrow ones (Figure 3). Moreover, highly regular 2D tmla domains with a superstructure oriented along the [011] high-symmetry substrate direction develop on all "wide" terraces, separating them topologically from those in the bunches, where irregular molecular aggregates occur. The ordered domains extend over whole terraces and, with the usual absence of domain walls, functionalize the *entire* terrace in a way that a regular homogenous tmla arrangement is exclusively found on a given terrace. Due to the spatial limitations of the scanner, the total extension of individual terraces cannot be unambiguously determined; however, within the accessible range of max. 2.37 μm^2 (1.54 μm x 1.54 μm), most of the "wide" terraces run continuously. Continuous terraces can reach 290 nm in width, but typical widths fall in the 100–200 nm range (estimated from an analysis of several large-scale topographs), whereas within the bunches dered two-dimensional organizations with a superstructure oriented along the Cu(100) high-symmetry direction exist. The local arrangement of the molecules for one type can be followed in Figure 4a: identically oriented tmla molecules, resolved here as three-lobe protrusions, are arranged in a well-ordered domain structure characterized by a (3×3) unit cell where individual molecules are separated by a distance of 7.65 Å in both perpendicular directions, coinciding with the Cu(100) azimuths. It is generally known for the STM imaging mode of small organic adsorbates on metal surfaces that the topography shows specific C–C bonds rather than positions of individual C atoms.[57] Having this in mind, and considering the imaged characteristic length of about 8 Å for individual molecules (Figure 4a), we can tentatively describe the imaged fea-

tures as carboxylic groups in a *para* geometry with *ortho* carboxylate moieties pointing towards the substrate and imaged as accompanying asymmetric protrusion. Such configuration is in line with the evidence from XPS analysis on the chemical state of molecular carboxylic groups. Notably, such a configuration and interpretation of the available STM data (a three-lobe appearance of tmla instead of the earlier proposed "four-lobes" interpretation[34]) effectively updates the previously suggested tentative scenario,[34] where the tmla species were proposed to adsorb in an essentially flat manner, similar to the conformation they adopt in low-temperature-deposited hydrogen-bonded multilayers. Furthermore, summing these observations (i.e. the tmla species with one deprotonated group anchoring to the substrate with *ortho* carboxylate moiety) with the NEXAFS data, which suggest a 25° out-of-normal tilt of the molecular plane in the adlayer, an intriguing chiral order in the molecular domain becomes apparent. The molecular model of the tmla adlayer, superimposed on the STM topograph of Figure 4a, gives a schematic representation of the chiral ordering in the tmla adlayer, essentially defined by the combination of the deprotonation-driven anchoring to the substrate through the *ortho* carboxylate moiety and the tilt of the molecular plane. Consequently, two domain types can be designated as *R* and *S* types (Figure 4).

This chiral ordering generally extends homogenously over the entire terraces. The boundaries between the domains in the organic-adlayer structure are extremely rare. An example is shown in the STM image of Figure 4b, where one can identify both chiral domains coexisting in a terrace, with the boundary running along the Cu[011] azimuth representing the mirror symmetry axis. The shift in molecular packing on the boundary (5.1 Å) arises from a misfit between molecular arrangements in each enantiomer. This observation also nicely confirms that the domains shown in Figure 4 are not related to STM imaging effects. The existence of azimuthally rotated domains is not excluded; however, because of the vast domain size, interdomain boundaries are extremely rare.

The tilted orientation and directional substrate anchoring of the tmla molecules suggest that lateral molecular interactions are decisive in the formation of the extended chiral domains. To reconcile the evidence obtained from XPS and NEXAFS studies on molecular chemical state and orientation with that obtained from the STM analysis, and to clarify the origin of the supramolecular ordering, DFT calculations were performed. The resulting model, explaining the essential features of all experimental evidence, is depicted in Figure 5. With a tmla *ortho* carboxylate group (marked as "a" in Figure 5a), coupled to the substrate by forming a Cu–carboxylate bond, and two carboxylic groups in *para* positions ("b" and "c"), interweaving the domain by H bonding and providing lateral correlation in the structure, the most stable configuration was obtained. The calculated tilt angle of the phenyl-ring plane with respect to the surface normal was 25°.

DFT results for the tmla–Cu surface carboxylate coupling are shown in Figure 6. The work function decreases (0.4 eV) upon adsorption. The overall bonding energy to the substrate is evaluated to be $E_b = 3.1$ eV. Such a large binding energy is understandable since the molecule adsorbs as a radical given that the hydrogen has been removed. Figure 6a shows the electron-density difference due to the adsorption of tmla on the substrate. The density shows the largest changes at the two oxygen atoms of tmla bonded to the surface and at the two nearest-neighbor copper atoms. The change is similar on both oxygen atoms, showing that they are similar; thus they are both in chemically equivalent states. The change shows a rearrangement of the charge density due to the adsorbate–substrate interaction on the oxygen atom. Figure 6b shows the change resulting from the interaction of two neighboring molecules. The hydrogen-bonding oxygen atoms experience an electron density increase along the hydrogen-bond axis and a decrease at the atomic site perpendicular to the bond axis, and the hydrogen atoms lose part of their electron density. Therefore, the interaction upon hydrogen bonding is mainly electrostatic, as it was seen in a similar previous study.[58] The effect along the longer hydrogen-bond axis close to the [011] direction is understandably weaker than that along the [011] direction. We found the lateral adsorbate–adsorbate interaction to be about 0.4–0.6 eV along the molecular lines by in-

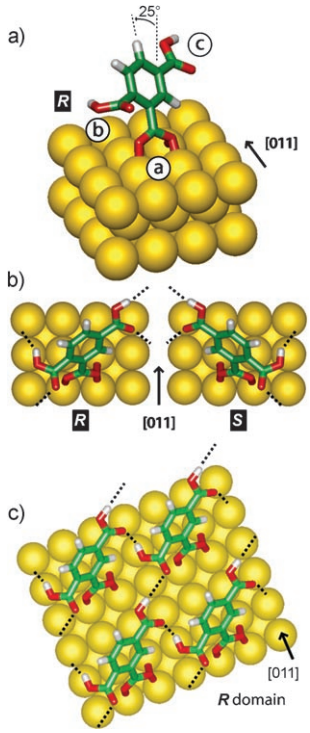

Figure 5. Chirality generation and propagation in a tmla adlayer viewed by DFT calculations. a) Details of chirality induction of tmla—with conformational restriction—shown for the *R*-enantiomer geometry upon molecular self-assembly. The copper–caboxylate bond, linking tmla to the substrate, is marked as "a"; the moieties "b" and "c" are engaged in intermolecular carboxylic–carboxylic hydrogen bonds. Carbon is represented in green, oxygen in red, hydrogen in white, substrate Cu atoms in yellow. The out-of-normal 25° tilt of the molecular plane is indicated. b) The mirror representation of the *R*-enantiomeric tmla conformation with respect to the Cu [011] azimuth generates the *S* chiral counterpart. Hydrogen bonds, locking the tmla molecules within the domain, are represented by black dashed lines. c) Enantiopure *R* domain stabilized by lateral inter-tmla H bonding (marked with black dashed lines) stabilizing a two-dimensional chiral motif.

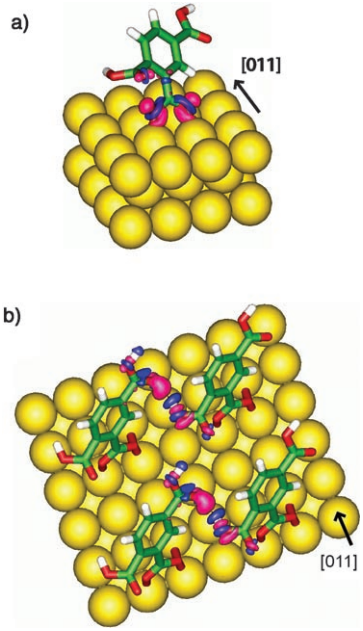

Figure 6. a) DFT calculation on the carboxylate anchoring of tilted monotrimellate on the Cu(100) substrate (the [011] direction is indicated). Electron-density differences n(tmla/Cu)−n(tmla)−n(Cu) at the Cu–carboxylate bonds are highlighted. b) Charge rearrangement as a result of hydrogen bonding quantified by the interaction density.[58] The contour levels are ±0.028 (a) and ±0.013 e^{-} $Å^{-3}$ (b); the colors indicate an increased (purple) and decreased (blue) electron density.

creasing the distance between the adsorbates in either of the molecular-chain directions. Such a charge redistribution can also result in a gradual shift of the involved oxygen species to lower binding energies in the XPS spectrum (see above).

The Cu–O bonding distances obtained from the DFT calculations are 2.09 and 2.03 Å, which are typical values for three-dimensional Cu–carboxylate compounds.[59] The pertaining surface core-level shifts are reproduced in Table 2. Given are the averages of the corresponding atoms, which have been shifted so that the phenyl C1 s and combined O_2 and O_3 peaks match with the experimental values. This is justified by the fact that the absolute DFT values are not precise due to the approximate exchange-correlation functional. The overall satisfactory agreement corroborates the model.

It is important to realize that the deprotonation of one carboxylic moiety alone (which often involves an upright adsorption geometry[37,38,60]) does not imply chirality induction of tmla. On the other hand, the molecules do not adopt a flat-lying conformation, which would be necessary to induce the chirality of prochiral species; instead, the upright-adsorbed tmla molecules preserve their mirror symmetry axis and can rotate around the C–C σ bond of the *ortho* group. However, the collective spatial arrangement, where the *para* carboxylic groups bind to the neighboring species via H bonding, inducing a correlated tilt of the tmla molecules (Figure 5 a), accounts for supramolecular chiral packing. Consequently, the intermolecular interactions, mediating the self-assembly, are the key to chirality induction in the organic domains.

Table 2. Comparison of experimental and calculated surface core-level shifts.

	DFT	Experiment
C1 s		
Phenyl	284.8	284.8
COO	287.2	287.6
COOH	288.0	288.9
O1 s		
COO	531.1	531.1
CO	531.6	532.2
OH	533.6	533.9

With the optimized geometry, the conformation of each individual molecule is effectively constrained to the surrounding: one conformational restriction is provided by the binding to the substrate and other two by the linkage to neighboring species. In Figure 5 a, this concept is graphically depicted. The out-of-normal tilt of the tmla molecules (25°) is the result of tmla–substrate bonding (Cu–carboxylate, marked by "a") and two carboxylic–carboxylic bonds (marked by "b" and "c") to the neighboring molecules, with an average H-bond length of ≈2 Å. Consequently, a chiral adsorption footprint of the conformed tmla with respect to the surface emerges and two enantiomeric tmla domains (*R* and *S*) can be distinguished by their mirror symmetry with respect to the substrate [011] azimuth (Figure 5 b). The optimized geometry of a hydrogen-bonded *R* domain is reproduced in Figure 5 c. The dominating H-bond feature is the lateral coupling of adjacent benzoic-acid groups where a bond length of 1.70 Å is estimated from the DFT results (Figure 6 b). Surprisingly, the dimerization motif of the carboxylic-acid moieties, typical for 3D carboxylic-acid aggregates and frequently occurring in 2D self-assembled layers, is suppressed; instead, the H···O distance of 2.77 Å along the molecular axis in the supramolecular layer indicates the presence of a comparatively weak hydrogen bond.[61,62] This feature reflects that the substrate coupling with its distinct carboxylate–Cu anchoring motif is the strongest interaction in the tmla layer.

The formed domains thus exemplify the induction of supramolecular chirality at the surfaces via noncovalent self-assembly of achiral molecular components. In contrast to previous studies, where the surface was used to induce 2D chirality of prochiral species or where enantiomorphic packing of flat-lying species occurred, with the present system the copper substrate—through an effective provision of a template for commensurate domain growth—supplies anchoring sites for the monotrimellate species and, by itself, does not define (or induce) chirality of the resulting assembly (contrasting with recently reported systems, where chiral signature arises upon specific molecule–substrate bonding[63,64]). For the latter, cooperative interaction phenomena in the self-assembly are responsible. Because the organic layers are quite robust (once formed they resist thermal annealing up to 480 K), these cooperative interactions are believed to be extremely effective, keeping the homochiral arrangement intact. An intriguing feature of this system is that the chiral signature can be changed by collective molecular rotations or tilt-angle flipping, whence the

energy barrier for *R*–*S* "switching" is expected to be relatively small.

The out-of-plane tilt and specific rotation of the molecular plane around the carboxylate C–C bond prevent from continuous transition between neighboring domains and indicate that a particularly strong lateral correlation of the tmla molecules exists within the domain, providing its substantial growth in size. The typical absence of domain boundaries on the entirety of a given surface terrace, leading finally to the development of homochiral *R* and *S* phases on the micrometer-sized surface areas, can be interpreted as follows: Whereas at elevated temperatures (450 K) molecular deposition results in the deprotonation of a carboxylic group and a possibly upright or random conformation of the tmla species, cooling down promotes spontaneous chiral resolution by the formation of H-bonded domains. It is likely that at a given monoatomic terrace, larger domains may consume smaller ones to minimize the energy of the system by reducing the domain boundaries. The whole process can be regarded as "spontaneous crystallization", in which a monodomain phase is energetically favorable.

In conclusion, mesoscopic chirality induction by supramolecular self-assembly of tmla on a Cu(100) surface is reported. Well-ordered structures evolve during molecular deposition on an elevated-temperature substrate, and two enantiomeric domain phases develop simultaneously at extended surface monoatomic terraces. Chirality induction upon molecular self-assembly is described by the conformational restriction of prochiral tmla in the structure of enantiopure domains: Two carboxylic functionalities of the molecule are involved in specific intermolecular H bonding, which results in a chiral motif due to a tilt of the molecular plane off the surface normal, whereas substrate anchoring is realized via copper–carboxylate bond formation. The appreciable substrate–adsorbate interaction induces changes in the surface morphology, which results in the formation of extended homochiral μm-scale terrace patterns. This can be regarded as a first step in a coordinated process (chiral-signature induction along with surface restructuring) to obtain potentially homochiral substrates.

Experimental Section

Sample Preparation: The experiments were performed in two ultrahigh vacuum (UHV) systems with a base pressure in the low 10^{-10} mbar region. Standard procedures of repeated cycles of Ar-ion bombardment (10 μA, 500 eV, 300 K, 20 min) and subsequent annealing (800 K, 15 min) were performed to obtain an atomically flat Cu(100) surface with regions showing monoatomic terraces of around 100 nm width. The cleanliness was monitored using XPS (in the case of XPS/NEXAFS experiments), and the surface was shown to be free from hydrocarbons and oxygen-containing species prior to the deposition experiments. In both preparation chambers, tmla was sublimated from powder (Sigma Aldrich, >99%) using a home-built Knudsen-type evaporation cell held at 415 K. Multilayer tmla deposition was carried out on the surface held at 120 K, with subsequent measurements performed at the same temperature. To achieve regular supramolecular monolayer domains (1 ML corresponds to a close-packed saturated organic layer), tmla was deposited with the substrate temperature kept at 450 K to increase surface mobility and allow for the chemical reactions necessary for the formation of well-ordered phases.

Scanning Tunneling Microscopy: The STM experiments were performed in situ, followed by a cool-down to room temperature. Molecular deposition rates were calibrated by area estimation from the STM images at (sub)monolayer coverages. The images were recorded at room temperature using a home-built VT-STM setup with typical tunneling conditions [$I = 0.5$ nA and V(sample) $= 1$ V].

XPS and NEXAFS Measurements: were performed in a UHV setup at the HE-SGM beam line at the Berlin synchrotron radiation facility BESSY II. The analysis chamber was equipped with a sputter gun, a quadrupole mass spectrometer, a twin-anode X-ray source, and a CLAM2 energy analyzer. All NEXAFS spectra were recorded in the partial electron yield (PEY) mode using a home-built electron detector based on a double-channel plate. For the energy calibration of each NEXAFS spectrum the photocurrent of a carbon-contaminated gold grid, with a characteristic peak at 284.9 eV, was recorded simultaneously with each spectrum. The energy scale was calibrated using the C1 s–π* transition of graphite at 285.4 eV. The gold grid was also used as a radiation-flux monitor. For the NEXAFS experiments the resolution was set to $\Delta E = 0.4$ eV at 300 eV. The C1 s NEXAFS raw data were normalized by a procedure consisting of several steps: First, the spectrum recorded for the clean substrate was multiplied by a correction factor, to yield equal intensities in the energy range 272–278 eV, and then subtracted. The resulting data were then corrected for the beam-line transmission by division through a spectrum obtained for a freshly sputtered gold wafer. Finally, the spectra were normalized to yield an edge jump (difference intensity between 275 and 325 eV) of one. The variation of the NEXAFS resonance intensities with the photon angle of incidence was used for the quantitative determination of the average tilt angle of the tmla molecules with respect to the surface normal. The analysis was performed according to the procedure described in the book by J. Stöhr.[65] Briefly, the average tilt angles of the tmla molecular plane are obtained using the following procedure: First, the intensity (area) of resonance #1 is determined for each angle. A plot of the intensity versus the angle of incidence for a vector-type orbital on a substrate with a more-than-threefold symmetry is created by plotting the curves for the different tilt angles (between 0 and 90 degrees) using a polarization factor of 0.82. The curves are calculated using formulas, which have been obtained by averaging over all azimuths, that is, the preferential azimuthal orientation is not considered. The intensities are normalized by only one free parameter until the best fit to one of the curves (corresponding to a certain tilt angle) of the diagram is obtained.

For the XPS measurements, the carbon 1 s and oxygen 1 s peaks were acquired with a beam energy of 400 and 650 eV, respectively. The pass energy of the analyzer was set at 50 eV. For the quantitative analysis, a complete set of XP spectra was acquired, in addition, with the Al K_α radiation of the lab source, with a pass energy set at 100 eV. Core-level photoemission spectra were fitted, with a number of component peaks and a background, using Voigt functions as line shapes of the individual components in the PeakFit software.

DFT Calculations: were performed with the generalized gradient approximation (GGA) of Perdew et al.[66] as the exchange-correlation functional in the Kohn–Sham equations.[67] The electronic wavefunctions were expanded in a plane-wave basis setup to a cutoff energy of 36 Ry, and the core–valence interaction was modeled with the ultrasoft pseudopotentials of Vanderbilt.[68] Three

substrate layers (the first one was relaxed with the adsorbate layer) together with 8 Å of vacuum were employed, and a (4×4) grid of Monkhorst–Pack[69] *k* points in the first Brillouin zone was used to approximate the integration over the reciprocal space. Simulated annealing- and geometry-optimization methods were used to find the optimal structure.

Keywords: chirality · density functional calculations · hydrogen bonds · photoelectron spectroscopy · scanning probe microscopy

[1] A. Ahmadi, G. Attard, *Langmuir* **1999**, *15*, 2420.
[2] J. D. Horvath, A. J. Gellman, *J. Am. Chem. Soc.* **2002**, *124*, 2384.
[3] D. S. Sholl, A. Asthagiri, T. D. Power, *J. Phys. Chem. B* **2001**, *105*, 4771.
[4] R. Fasel, M. Parschau, K.-H. Ernst, *Angew. Chem.* **2003**, *115*, 5336; *Angew. Chem. Int. Ed.* **2003**, *42*, 5178.
[5] V. Humblot, S. Haq, C. Muryn, W. A. Hofer, R. Raval, *J. Am. Chem. Soc.* **2002**, *124*, 503.
[6] A. Kühnle, T. R. Linderoth, B. Hammer, F. Besenbacher, *Nature* **2002**, *415*, 891.
[7] G. P. Lopinski, D. D. Wayner, R. A. Wolkow, *Nature* **2000**, *406*, 48.
[8] M. O. Lorenzo, C. J. Baddeley, C. Muryn, R. Raval, *Nature* **2000**, *404*, 376.
[9] P. Nassoy, M. Goldmann, O. Bouloussa, F. Rondelez, *Phys. Rev. Lett.* **1995**, *75*, 457.
[10] D. Stacchiola, L. Burkholder, W. T. Tysoe, *J. Am. Chem. Soc.* **2002**, *124*, 8984.
[11] R. Fasel, J. Wider, C. Quitmann, K.-H. Ernst, T. Greber, *Angew. Chem.* **2004**, *116*, 2913; *Angew. Chem. Int. Ed.* **2004**, *43*, 2853.
[12] Q. Chen, N. V. Richardson, *Nat. Mater.* **2003**, *2*, 324.
[13] J. V. Barth, J. Weckesser, G. Trimarchi, M. Vladimirova, A. D. Vita, C. Cai, H. Brune, P. Günter, K. Kern, *J. Am. Chem. Soc.* **2002**, *124*, 7991.
[14] S. D. Feyter, P. C. M. Grim, M. Rücker, P. Vanoppen, C. Meiners, M. Sieffert, S. Valiyaveettil, K. Müllen, F. C. D. Schryver, *Angew. Chem.* **1998**, *110*, 1281; *Angew. Chem. Int. Ed.* **1998**, *37*, 1223.
[15] S. d. Feyter, A. Gesquiere, K. Wurst, D. B. Amabilino, J. Veciana, F. C. d. Schryver, *Angew. Chem.* **2001**, *113*, 3317; *Angew. Chem. Int. Ed.* **2001**, *40*, 3217.
[16] C. B. France, B. A. Parkinson, *J. Am. Chem. Soc.* **2003**, *125*, 12712.
[17] R. Viswanathan, J. A. Zasadzinski, D. K. Schwartz, *Nature* **1994**, *368*, 440.
[18] J. Weckesser, A. D. Vita, J. V. Barth, C. Cai, K. Kern, *Phys. Rev. Lett.* **2001**, *87*, 096101.
[19] D. G. Yablon, D. Wintgens, G. W. Flynn, *J. Phys. Chem. B* **2002**, *106*, 5470.
[20] M. Schunack, E. Laegsgaard, I. Stensgaard, I. Johannsen, F. Besenbacher, *Angew. Chem.* **2001**, *113*, 2693; *Angew. Chem. Int. Ed.* **2001**, *40*, 2623.
[21] J. I. Pascual, J. V. Barth, G. Ceballos, G. Trimarchi, A. D. Vita, K. Kern, H.-P. Rust, *J. Chem. Phys.* **2003**, *120*, 11367.
[22] M. Parschau, S. Romer, K.-H. Ernst, *J. Am. Chem. Soc.* **2004**, *126*, 15398.
[23] J. A. Switzer, H. M. Kothari, P. Poizot, S. Nakanishi, E. W. Bohannan, *Nature* **2003**, *425*, 490.
[24] L. Pérez-Garcìa, D. B. Amabilino, *Chem. Soc., Rev.* **2002**, *31*, 342.
[25] V. Humblot, S. M. Barlow, R. Raval, *Prog Surf. Sci.* **2004**, *76*, 1.
[26] S. Stepanow, N. Lin, F. Vidal, A. Landa, M. Ruben, J. V. Barth, K. Kern, *Nano Lett.* **2005**, *5*, 901.
[27] K. Biradha, D. Dennis, V. MacKinnon, C. V. K. Sharma, M. J. Zaworotko, *J. Am. Chem. Soc.* **1998**, *120*, 11894.
[28] S. Clair, S. Pons, A. P. Seitsonen, H. Brune, K. Kern, J. V. Barth, *J. Phys. Chem. B* **2004**, *108*, 14585.
[29] M. Lackinger, S. Griessl, T. Markert, F. Jamitzky, W. M. Heckl, *J. Phys. Chem. B* **2004**, *108*, 13652.
[30] M. Lingenfelder, H. Spillmann, A. Dmitriev, S. Stepanow, N. Lin, J. V. Barth, K. Kern, *Chem. Eur. J.* **2004**, *10*, 1913.
[31] S. Stepanow, T. Strunskus, M. Lingenfelder, A. Dmitriev, H. Spillmann, N. Lin, J. V. Barth, C. Wöll, K. Kern, *J. Phys. Chem. B* **2004**, *108*, 19392.
[32] P. Messina, A. Dmitriev, N. Lin, H. Spillmann, M. Abel, J. V. Barth, K. Kern, *J. Am. Chem. Soc.* **2002**, *124*, 14000.
[33] H. Spillmann, A. Dmitriev, N. Lin, P. Messina, J. V. Barth, K. Kern, *J. Am. Chem. Soc.* **2003**, *125*, 10725.
[34] A. Dmitriev, H. Spillmann, N. Lin, J. V. Barth, K. Kern, *Angew. Chem. Int. Ed.* **2003**, *115*, 2774; *Angew. Chem. Int. Ed.* **2003**, *42*, 2670.
[35] A. Dmitriev, H. Spillmann, M. Lingenfelder, N. Lin, J. V. Barth, K. Kern, *Langmuir* **2004**, *20*, 4799.
[36] S. Stepanow, M. Lingenfelder, A. Dmitriev, H. Spillmann, E. Delvigne, N. Lin, X. Deng, C. Cai, J. V. Barth, K. Kern, *Nat. Mater.* **2004**, *3*, 229.
[37] D. S. Martin, R. J. Cole, S. Haq, *Phys. Rev. B* **2002**, *66*, 155427.
[38] A. Dmitriev, N. Lin, J. Weckesser, J. V. Barth, K. Kern, *J. Phys. Chem. B* **2002**, *106*, 6907.
[39] L. H. Dubois, B. R. Zegarski, R. G. Nuzzo, *Langmuir* **1986**, *2*, 412.
[40] C. A. Fustin, R. Gouttebaron, C. D. Nadai, R. Caudano, F. Zerbetto, D. A. Leigh, P. Rudolf, *Surf. Sci.* **2001**, *474*, 37.
[41] S. W. Han, S. W. Joo, T. H. Ha, Y. Kim, K. Kim, *J. Phys. Chem. B* **2000**, *104*, 11987.
[42] A. D. Vogt, T. Han, J. T. P. Beebe, *Langmuir* **1997**, *13*, 3397.
[43] M. Wühn, J. Weckesser, C. Wöll, *Langmuir* **2001**, *17*, 7605.
[44] J. M. Rynkowski, S. Affrossman, J. M. R. MacAllister, R. A. Pethrick, *Surf. Sci.* **1987**, *182*, 1.
[45] F. Takusagawa, K. Hirotsu, A. Shimada, *Bull. Chem. Soc., Jap.* **1973**, *46*, 2960.
[46] G. Iucci, V. Carravetta, P. Altamura, M. V. Russo, G. Paolucci, A. Goldoni, *Chem. Phys.* **2004**, *302*, 43.
[47] T. Bitzer, N. V. Richardson, S. Reiss, M. Wühn, C. Wöll, *Surf. Sci.* **2000**, *458*, 173.
[48] B. Immaraporn, P. Ye, A. J. Gellman, *J. Phys. Chem. B* **2004**, *108*, 3504.
[49] B. Parker, B. Immaraporn, A. J. Gellman, *Langmuir* **2001**, *17*, 6638.
[50] K. Weiss, S. Gebert, M. Wühn, H. Wadepohl, C. Wöll, *J. Vac. Sci. Technol.* **1998**, *16*, 1017.
[51] S. Haq, F. M. Leibsle, *Surf. Sci.* **1996**, *355*, L345.
[52] F. Rosei, M. Schunack, P. Jiang, A. Gourdon, E. Laegsgaard, I. Stensgaard, C. Joachim, F. Besenbacher, *Science* **2002**, *296*, 328.
[53] X. Zhao, *J. Am. Chem. Soc.* **2000**, *122*, 12584.
[54] F. S. Tautz, M. Eremtchenko, J. A. Schaefer, M. Sokolowski, V. Shklover, K. Glöckler, E. Umbach, *Surf. Sci.* **2002**, *502–503*, 176.
[55] X. Zhao, Z. Gai, R. G. Zhao, W. S. Yang, T. Sakurai, *Surf. Sci.* **1999**, *424*, L347.
[56] Q. Chen, N. V. Richardson, *Prog Surf. Sci.* **2003**, *73*, 59.
[57] P. Sautet, *Chem. Rev.* **1997**, *97*, 1097.
[58] A. P. Seitsonen, Y. J. Zhu, K. Beduerftig, H. Over, *J. Am. Chem. Soc.* **2001**, *123*, 7347.
[59] R. C. Mehrotra, R. Bohra, *Metal Carboxylates*, Academic Press, London, **1983**.
[60] B. G. Frederick, Q. Chen, F. M. Leibsle, M. B. Lee, K. J. Kitching, N. V. Richardson, *Surf. Sci.* **1997**, *394*, 1.
[61] T. Steiner, *Angew. Chem.* **2002**, *114*, 50; *Angew. Chem. Int. Ed.* **2002**, *41*, 48.
[62] G. Desiraju, *Acc. Chem. Res.* **1996**, *29*, 441.
[63] V. Humblot, M. O. Lorenzo, C. J. Baddeley, S. Haq, R. Raval, *J. Am. Chem. Soc.* **2004**, *126*, 6460.
[64] A. Mulligan, I. Lane, G. B. D. Rousseau, S. M. Johnston, D. Lennon, M. Kadodwala, *Angew. Chem.* **2005**, *117*, 1864; *Angew. Chem. Int. Ed.* **2005**, *44*, 1830.
[65] J. Stöhr, *NEXAFS Spectroscopy*, Springer-Verlag, Berlin, Heidelberg, **1992**.
[66] J. P. Perdew, J. A. Chevary, S. H. Vosko, K. A. Jackson, M. R. Pederson, D. J. Singh, C. Fiolhais, *Phys. Rev. B* **1992**, *46*, 6671.
[67] The calculations were performed with the program VASP: G. Kresse, J. Furthmüller, *Comput. Mater. Sci.* **1996**, *6*, 15; G. Kresse, J. Furthmüller, *Phys. Rev. B* **1996**, *54*, 11169.
[68] D. Vanderbilt, *Phys. Rev. B* **1990**, *41*, 7892.
[69] H. J. Monkhorst, J. D. Pack, *Phys. Rev. B* **1976**, *13*, 5188.

Received: February 23, 2006
Revised: June 8, 2006
Published online on September 6, 2006

